Differences in brain networks during consecutive swallows detected using an optimized vertex-frequency algorithm

Iva Jestrović[a], James L. Coyle[b], Ervin Sejdić[a,*]

[a] *Department of Electrical and Computer Engineering, Swanson School of Engineering, University of Pittsburgh, Pittsburgh, PA 15261, USA*
[b] *Department of Communication Science and Disorders, School of Health and Rehabilitation Sciences, University of Pittsburgh, Pittsburgh, PA 15260, USA*

*Ervin Sejdić is the corresponding author. Mailing address: Department of Electrical and Computer Engineering, Swanson School of Engineering, University of Pittsburgh, Pittsburgh, PA, 15261, USA. Tel: +1-412-624-0508.
Email address: esejdic@ieee.org (Ervin Sejdić)

Abtract

Patients with dysphagia can have higher risks of aspiration after repetitive swallowing activity due to the "fatigue effect". However, it is still unknown how consecutive swallows affect brain activity. Therefore, we sought to investigate differences in swallowing brain networks formed during consecutive swallows using a signal processing on graph approach. Data was collected from 55 healthy people using electroencephalography (EEG) signals. Participants performed dry swallows (i.e., saliva swallows) and wet swallows (i.e., water, nectar-thick, and honey thick swallows). After standard pre-processing of the EEG times series, brain networks were formed using the time-frequency based synchrony measure, while signals on graphs were formed as a line graph of the brain networks. For calculating the vertex frequency information from the signals on graphs, the proposed algorithm was based on the optimized window size for calculating the windowed graph Fourier transform and the graph S-transform. The proposed algorithms were tested using synthetic signals and showed improved energy concentration in comparison to the original algorithm. When applied to EEG swallowing data, the optimized windowed graph Fourier transform and the optimized graph S-transform showed that differences exist in brain activity between consecutive swallows. In addition, the results showed higher differences between consecutive swallows for thicker liquids.

Keywords: Swallowing, dysphagia, electroencephalography, graph signal processing, vertex-frequency analysis.

Introduction

Dysphagia refers to any kind of swallowing disorder (Logemann, 1998), and it commonly occurs due to neurological conditions, such as stroke (Gottlieb et al., 1996), Parkinson's diseases (Murray, 1999), cerebral palsy (Rogers et al., 1994), or brain injuries (Lazarus and Logemann, 1987). These neurological conditions can cause lesions in the disparate cortical and subcortical brain regions (Smithard et al., 1996), which are responsible for dysphagia (Cichero and Murdoch, 2006; Robbins and Levine, 1988; Veis and Logemann, 1985). Besides difficulty swallowing, patients who are suffering from dysphagia can develop other medical conditions, such as malnutrition (Curran, 1992), dehydration (Smithard et al., 1996), or immune system failure (Curran and Groher, 1990). A major consequence of dysphagia is the compromised operation of airway protection, which puts these patients at a high risk of aspiration (Langmore et al., 1998; Ramsey et al., 2003). Aspiration can develop into pneumonia, which according to previous studies, results in death for 20% to 50% of pneumonia sufferers (Pugliese and Lichtenberg, 1987; Garibaldi et al., 1981; Bryan and Reynolds, 1984).

Although highly simplified, the following is a brief review of the neuroanatomical substrates involved in swallowing. In general the oral preparatory stage and initiation of the oral transit stage are principally under volitional control, with numerous active supra- and infratentorial regions including bilateral cortical and subcortical, frontal, prefrontal and parietal regions, and a pontomedullary ?swallowing center?. During oral preparation, the cricopharyngeal portion of the inferior constrictor, which is the inferior-most region of the pharynx and the portal to the esophagus, is tonically closed with an average resting intraluminal pressure of between 100-150mmHg though there is much variability (Bhatia and Shah, 2013). At the onset of oral propulsion of the masticated (or liquid) bolus in a healthy young subject, the summation of all kinesthetic, and general and sensory afferent input to the swallowing, lead to vagal inhibition of some of the tonic closure of the CP though it remains closed. Immediately thereafter, traction forces are delivered to the hyoid-larynx complex via contraction of suprahyoid musculature which distends the CP segment, while the reflexive peristaltic superior-inferior collapse of the pharyngeal tube occurs due to pharyngeal constrictor and lingual compression. constrictor.

Electrophysiologic studies have elucidated much of the neuroanatomical underpinnings of swallowing function though much remains poorly understood (Jestrović et al., 2015). Numerous hemispheric structures, when directly stimulated, generate discrete facial, lingual and mandibular movements that are not integrated into a swallow sequence. Likewise, the combined and coordinated mandibular, facial, pharyngeal and laryngeal actions occurring actual mastication-swallowing patterns can be elicited through electrical stimulation. Prefrontal microeletrode stimulation has been show to produce specific contractions of muscles responsible for movement of these structures, while more current delivered through larger electrodes has been shown to produce the coordinated pharyngeal swallow response (Miller, 1986). Similarly, stimulation of corticobulbar and subthalamic regions adjacent to the substantia nigra and midbrain reticular formation regions have been

shown to also elicit a a masticatory-swallow response.

Reflexive swallowing on the other hand occurs typically with little to no oral preparatory and transit stages, and involve primarily infratentorial structures. Early research into these deep brain regions and their relationship to swallowing suggests that autonomic and other visceral and somatic responses integrate with one another and summate to produce the reflexive swallow as well as esophageal activity (Bieger, 1993). Therefore these higher level centers appear to be involved in acquisition of feeding and swallowing behaviors and related motor learning.

However infratentorial, brainstem regions strongly mediate the activation and propagation of the coordinated swallow response. General sensory input through trigeminal, glossopharyngeal and vagal nerves, and gustatory input through facial and glossopharyngeal nerves from the periphery, directly and indirectly (via trigeminal pathways) deliver the necessary kinesthetic, taste, proprioceptive and tactile input to the nucleus and tractus solitarius, the sensory epicenter of swallowing activity. Electrical stimulation of pontine areas adjacent to the trigeminal motor nucleus evoke mastication and swallowing while destruction of the dorsolateral medulla, as seen in vertebral artery occlusion and posterior inferior cerebellar artery syndromes like the lateral medullary or Wallenberg syndrome, is well-known to produce the clinical syndrome of dysphagia characterized by an absent pharyngeal response, failure of inhibition of CP tonic closure which increases inertia at the entrance to the esophagus, and pharyngeal and laryngeal paralysis, with preserved buccofacial and masticatory behavior.

This same medullary region, containing portions of the reticular formation and adjacent nucleus and tractus solitarius (the principal sensory nucleus receiving vagal general afferent and special sensory information from the oropharyngeal mechanism) and nucleus ambiguus (the principal motor nucleus activating the pharyngeal, laryngeal and esophageal structures innervated by the 9th and 10th cranial nerves), and surrounding structures, has been referred to as the medullary swallowing center (Sang and Goyal, 2001). Interestingly, unilateral dorsolateral medullary damage has been shown to produce contralateral sensorimotor impairments and bilateral swallowing disconnection syndromes (Aydogdu et al., 2001).

The majority of the preceding simplified scheme of swallowing function, focuses on peripheral activation patterns though much evidence exists indicating significant hemispheric activity, and as a result, much research into swallowing rehabilitation has likewise focused on manipulation of peripheral structures. In order to provide a better rehabilitation strategy, it is important to also understand central swallowing neurophysiology and the neural functions underlying conditions that could increase the risk of aspiration for dysphagic patients (Jestrović et al., 2015). Studies have shown that in comparison to individual, discrete single swallows, consecutive swallows which many people perform naturally, demonstrate altered and variable swallowing control for people who have impaired clearance of swallowed material from the throat due to sensorimotor impairments affecting swallowing control (Plaxico and Loughlin, 1981; Dusick, 2003; Ney et al.,

2009; Solomon, 2006; Molfenter and Steele, 2013; Eisbruch et al., 2002). There are many reasons for this trend in consecutive swallows, such as: various patterns of post-swallow residue in the pharynx, inefficient propulsion of the bolus by the tongue into the pharynx and esophagus, all of which may be explained by phenomena such as progressive fatigue or attenuated activation of the muscles of the aerodigestive tract involved in swallowing. Therefore, the investigation of the differences in neural activation between the individual swallows within sequences of consecutive swallows could lead to a better understanding of swallowing neurology and produce swallowing therapy options that exploit understanding of central processing of swallowing for patients with dysphagia. Previous studies showed that the brain's plasticity enables reorganization of the sensory and motor cortex (Rosenkranz et al., 2008; Davenport et al., 2011; Robbins et al., 2008). This reorganization is correlated with the rehabilitation of patients, who are suffering from some neurological conditions, such as stroke (Hamdy et al., 2000; Doeltgen and Huckabee, 2012). This leads us to speculate that the analysis of swallowing and swallowing disorders from a brain activity perspective could yield useful insights into how to exploit this reorganization to better rehabilitate neurogenic dysphagia. Therefore, the analysis of differences in brain activity between consecutive swallows is of particular interest.

The graph theory approach is widely used technique for analyzing brain organization from the EEG signals (Eguiluz et al., 2005; Kaiser and Hilgetag, 2004; Micheloyannis et al., 2006; Sporns and Zwi, 2004). Vertices (i.e., nodes) represent brain regions of interest, edges (i.e., connections between vertices) represent synchronization between those brain regions. By analyzing the connective relationships between and among neighborhoods of vertices, we aim to provide information about topological properties of the network which can lead to better understanding of the brain activity during swallowing. In the recent years, there is an increased need for gaining additional information beyond architectural graph structures. Deeper insights into brain networks formed from EEG recordings can be accomplished using the signal processing on graphs approach (Shuman et al., 2013a; Narang and Ortega, 2013; Leonardi and Van De Ville, 2013). In other words, besides information about position of the vertices and the connections between them, each vertex can contain additional observations that forms a signal on graph. Signal processing on graphs enables the spectral analysis of signals associated with a brain network. More precisely, using vertex-frequency tools it is possible to extract information about signal frequency changes in multiple brain regions of interest. This approach provides information about low frequency components that describe slowly changing brain signals, as well as high frequency components representing fast changes in brain signals. Previous studies showed that slow and fast changing brain signals are important for describing various neurological behaviors and diseases (Garrett et al., 2012; Heisz et al., 2012). Thus, signal processing on graphs is a valuable clinical tool to detect anomalies in graphs (Sun et al., 2005; Noble and Cook, 2003; Eberle and Holder, 2007). In our previous study, we developed an algorithm for calculating a fast windowed graph Fourier transform ($FWGFT$) and a fast graph S-transform ($FGST$) (Jestrović et al., 2017). In the same study, we showed

that vertex-frequency representations (graph signal processing equivalents of time-frequency representations (Sejdić et al., 2009)) of the brain network during healthy swallowing has a distinctive pattern. Therefore, we believe that vertex-frequency information from the signals on each swallowing brain network can individually provide unique information, which enables the analysis of the differences between consecutive swallows.

Even though $FWGFT$ and $FGST$ are shown to be good tools for extracting vertex-frequency information from each swallowing brain network, they suffer from some drawbacks. $FWGFT$ has limitations regarding the fixed window size. Choosing too wide or too narrow window can result in poor resolution of the representation of the graph's frequency content. On the other hand, $FGST$ in some cases suffers from bad energy concentration in the vertex-frequency representation. One way to optimize window size with the windowed graph Fourier transform and the graph S-transform is to directly optimize energy concentration in order to minimize the spread of the energy beyond the edges of the signal components (Sejdić et al., 2008). When applied to the swallowing brain network, the optimized algorithm could provide more reliable information about the differences in vertex-frequency representations of the swallowing brain network between consecutive swallows.

We hypothesized that brain networks are different between consecutive swallows. Investigating brain activity during the active use of the muscles involved in swallowing could explain if decreased swallowing control is due to changes in the muscles' activation that are produced by fatigue or due to changes in the muscles' activation controlled by the brain. Neurological conditions that cause the brain damages, which are responsible for dysphagia, may also affect the regions of the brain, which are responsible for the control of extensive muscle activation. In order to provide the best results, we also introduced a method based on the concentration measure, which calculates the optimal window for extracting frequency information from signals on a graph. Calculating an optimal window size automatically will enable a more efficient extraction of the frequency content from the graphs formed during swallowing, as well as, provide the best vertex-frequency resolution.

Fast windowed graph Fourier transform and fast graph S-transform

In our previous work, we developed a fast algorithm for calculating windowed graph Fourier transform ($FWGFT$) and fast graph S-transform ($FGST$). $FWGFT$ and $FGST$ evaluate vertex-frequency information from the graph signals by operating on the spectra of the graph signal and spectra of the window function.

In order to define windowed graph Fourier transform from the classical signal processing to the graph settings, we first define the Laplasian matrix from the each graph (Hammond et al., 2011; Narang and Ortega, 2012). The graph Laplacian is defined as $\mathcal{L} := \mathcal{D} - \mathcal{W}$, where $\mathcal{D}$ is diagonal degree matrix. Then we define eigenvectors of the graph Laplacian ($\{\mathcal{X}_l\}_{l=0,1,\ldots,N-1}$), and eigenvalues $\{\lambda_l\}_{l=0,1,\ldots,N-1}$. Each eigenvector

corresponds to the one eigenvalue, which means that in signal processing on graph settings eigenvalues will correspond to the signal on the graph's frequency.

$FWGFT$ and $FGST$ are calculated by applying the inverse graph Fourier transform of the α domain, where the α domain is the Fourier transform of the windowed Fourier transform. According to the previous study, the α domain can be represented as multiplication of the signal spectra shifted by each frequency point with the spectra of the window function (Jestrović et al., 2017). We can write alpha domain as:

$$\alpha(l', l) = \hat{f}(l' + l) \cdot \hat{w}(l), \tag{1}$$

where $\hat{f}$ is the spectra of the graph signal and $\hat{w}$ is the spectra of the window function, while l and l' refer to the graph signal frequency. In the case of the $FWGFT$, the window function is defined directly in the spectral domain as a heat kernel $\hat{w}(\lambda_l) = Ce^{-k\lambda_l}$, where k is arbitrarily chosen such that the vertex-frequency representation has the most optimal resolution, and C is chosen such that $||\hat{w}||_2 = 1$. In the case of the $FGST$, the window function is defined in the vertex domain as $w(n) = \frac{|\lambda_l|}{\sqrt{2\pi}} e^{\frac{n^2\lambda_l^2}{2}}$. Finally, we calculate windowed graph Fourier transform by taking the inverse Fourier transform from each frequency level of the α domain:

$$Sf(i, l) = \sum_{l'=1}^{N} \alpha(l', l)\mathcal{X}_l(i), \tag{2}$$

where i refers to the node and l is the signal frequency which corresponds to the eigenvalues λ_l of the graph Laplacian.

The proposed scheme

The windowed graph Fourier transform has a limitation regarding the fixed window size. A poor window size choice can result in an unacceptable resolution of the frequency content representation. For $\hat{w}(\lambda_l) = Ce^{-k\lambda_l}$, the window size depends on the parameter k (i.e., as k will tend to be more narrow). On the other hand, improvement of the energy concentration with the graph S-transform could be done by introducing a new parameter p into the window function. Thus, the new window function used in the graph S-transform would be defined as $w(i) = \frac{|\lambda_l|^p}{\sqrt{2\pi}} e^{\frac{i^2\lambda_l^{2p}}{2}}$, where parameter p will be optimized. In order to automatically calculate an optimal window size, concentration measure (CM) (Stanković, 2001) was used.

CM is defined as:

$$CM(\tau) = \frac{1}{\sum_{i=0}^{N-1}\sum_{l=1}^{N} |S^\tau f(i, l)|} \tag{3}$$

where $S^\tau f(i, l)$ is the vertex-frequency representation and τ is the parameter, which we want to optimize. In the case of $FWGFT$, τ will be k, while in the case of $FGST$, τ will be p. Optimal τ can be calculated as a vertex-invariant constant or as a vertex dependent parameter ($\tau(i)$). In the following subsections both algorithms are described.

Algorithm for optimizing vertex-invariant τ

To calculate the optimal value for the parameter τ, we will have to calculate the vertex-frequency representation using different values of τ ($S^{\tau}f(i,l)$). In the next step, each calculated vertex-frequency representation will be normalized, in order to provide equal energy:

$$\overline{S^{\tau}f(i,l)} = \frac{S^{\tau}f(i,l)}{\sqrt{\sum_{i=0}^{N-1}\sum_{l=1}^{N}|S^{\tau}f(i,l)|^2}}. \tag{4}$$

Using equation (3), concentration measures will be calculated for each normalized vertex-frequency representation:

$$CM(\tau) = \frac{1}{\sum_{i=0}^{N-1}\sum_{l=1}^{N}|\overline{S^{\tau}f(i,l)}|}. \tag{5}$$

In addition, the optimal parameter τ, will be determined as:

$$\tau_{opt} = \max_{\tau}[CM(\tau)]. \tag{6}$$

Algorithm for optimizing vertex-dependent $\tau(i)$

In the first step, we will calculate the vertex-frequency representation of the signal using the formula described in the Section b, and from that vertex-frequency representation we will calculate the energy E. Then, the vertex-frequency representations will be calculated by using the different values of τ ($S^{\tau}f(i,l)$). Vertex-frequency representations will be normalized as:

$$\overline{S^{\tau}f(i,l)} = \sqrt{E}\frac{S^{\tau}f(i,l)}{\sqrt{\sum_{i=0}^{N-1}\sum_{l=1}^{N}|S^{\tau}f(i,l)|^2}}. \tag{7}$$

The concentration measure that corresponds to each vertex will be calculated as:

$$CM(i,\tau) = \frac{1}{\sum_{l=1}^{N}|\overline{S^{\tau}f(i,l)}|}. \tag{8}$$

Finally, the optimal $\tau(i)$ for the each vertex will be the maximized concentration measure:

$$\tau_{opt} = \arg\max_{\tau}[CM(i,\tau)]. \tag{9}$$

Performance evaluation of the optimized vertex-frequency algorithms

The algorithms were evaluated using the test graph signals, where the expected frequency was known. As a test signal, we used a time series as the path graph, where each time point represents nodes on the

graph and time samples are signals on the graph. The weights of the edges between nodes are equal to one. The test signals s_1 and s_2 are defined as (see Figure 1):

$$s_1(n) = \begin{cases} \cos(15\pi \ln((10n-10.5)^2+1)) & 0 \le n < 100 \\ \cos(15\pi \ln((10n-10.5)^2+1)) + \cos(200\pi n) & 100 \le n < 180 \\ \cos(15\pi \ln((10n-10.5)^2+1)) & 180 \le n \le 200 \end{cases} \tag{10}$$

$$\begin{aligned} s_2(n) &= \cos\left[40\pi(n-0.5)\arctan(21n-10.5) - 20\pi\ln((21n-10.5)^2+1)/21\right] \\ &+ \sin(\pi(80n-kn^2)) \end{aligned} \tag{11}$$

Next, we calculated $FWGFT$, $FGST$, optimized $FWGFT$, and the optimized $FGST$. For calculating optimized $FWGFT$ as a value of k we used a range of values from 10 to 70 with increments of 1, while the k parameter was equal to 35 for calculating the $FWGFT$ defined in (2). For calculating the optimized $FGST$s, a range of p values from 0.01 to 1 with increments of 0.01 were used. Vertex-frequency representations for the test signals s_1 and s_2 are presented in Figures 2 and 3 respectively.

The concentration measure algorithm showed that the optimal k value for calculating $FWGFT$ for s_1 is equal to 25, while for calculating $FWGFT$ for s_2, it is equal to 5. Also, the concentration measure algorithm showed that the optimal p value for calculating $FGST$ for s_1 is equal to 0.57, while for calculating $FGST$ for s_2 is equal to 0.79. Improvements in the representation of the optimized algorithm can be clearly seen between Figures 2 and 3. The performance measure of each representation was calculated using the formula:

$$\Xi = \left(\sum_{i=0}^{N-1} \sum_{k=1}^{N} |\overline{S^\tau f(i,k)}| \right)^{-1}, \tag{12}$$

where $|\overline{S^\tau f(i,k)}|$ is the normalized vertex-frequency representation. This performance formula is actually a concentration of the vertex-frequency representation. In addition, the performance measure is also estimated for the signals on graph contaminated with the noise (SNR=$10dB$ and SNR=$20dB$). We have calculated 100 iterations of each algorithm when signals are contaminated with 10dB of noise, and when contaminated with 20dB of noise. Then, we have examined statistical differences amongst all combinations of the standard $FWGFT$, the vertex-invariant optimized $FWGFT$, the vertex-dependent optimized $FWGFT$, the standard $FGST$, the vertex-invariant optimized $FGST$, and the vertex-dependent optimized $FGST$. The results of the performance measure for each vertex-frequency representation for both signals are shown in Table 1. According to Table 1, the performance measure value does not show improvement for the optimized algorithms when it is used for the $FWGFT$. However, the $FGST$ performance measure value is the highest for each representation that used vertex-invariant optimized window size. Table 1 shows that with the higher level of noise, the performance measure value tends to be lower. Also, the Wilcoxon rank-sum statistical test

(Wilcoxon et al., 1963) showed significant statistical differences between results obtained with each algorithm for each SNR level ($p << 0.01$).

Experimental procedure

55 healthy people, between the ages of 18 and 25, participated in the data collection process. The protocol was approved by the Institutional Review Board at the University of Pittsburgh. The EEG signals were collected from 64 EEG electrodes, which were positioned according to the 10-20 international electrode system (Jasper, 1958) provided by the actiCAP active electrodes EEG cap (BrainProducts, Germany). The EEG signals were amplified using the actiCHamp amplifier (BrainProducts, Germany). The P1 electrode was chosen as a reference. The electrodes' impedance during the testing was below 15 kΩ. The data was saved using the PyCorder acquisition software, which also provided a 10 kHz sampling frequency. During the EEG recordings, the swallowing vibrations were simultaneously recorded using a dual-axis accelerometer positioned on the anterior side of the patient's neck. The swallowing vibrations provided segmentation start and stop points for each swallow. Swallowing segmentation with the dual-axis accelerometer is described in detail in one of our previous studies (Jestrović et al., 2013). After setting-up devices for data acquisition, the participants were asked to perform five saliva swallows, five water swallows, five nectar-thick apple juice swallows (nectar-thick, Nestlé Health Care Inc., Florham Park, N.J.), and then five honey-thick apple juice swallows (honey-thick, Nestlé Health Care Inc., Florham Park, N.J.) The unit for measuring viscosity was centipoise (cP), where 1 cP corresponds to the viscosity of water. The nectar-thick apple juice with a viscosity of 150cP is considered mildly thick, while the honey-thick apple juice with a viscosity of 400cP is considered moderately thick. The water, nectar, and honey were served chilled (3-5C) in separate cups. Since previous studies documented differences in comfortable bolus size between sex (Adnerhill et al., 1989), the bolus size were not measured. However, participants were instructed to consume a comfortable amount of bolus volume.

Pre-processing steps, forming graphs and signals on graphs

The collected data was further pre-processed with the EEGlab MATLAB toolbox (Delorme and Makeig, 2004). All of the signals were downsampled to 256 Hz, then this result was band-pass filtered from 0.1 Hz to 100 Hz with elliptical IIR filter. In order to remove the noise associated with the power supply, all of the signals were filtered with an elliptical notch filter with cut-off frequencies at 58 Hz to 62 Hz. In the next step, the signals were segmented on separate swallows according to the segmentation points provided by the accelerometer signal. The segmented swallows are then visually inspected for the presence of artifacts. All presented artifacts were removed using the independent component analysis (ICA) (Hyvärinen and Oja, 2000) algorithm. The EEG data samples, which had unreasonable values due to some specific artifact (i.e.

electrode lost connection) which could not be removed by ICA, were excluded from the study. Less than 5% of the EEG data samples were excluded.

The weighted connectivity networks are formed using the time-frequency based phase synchrony measure proposed by Aviyente et al (Aviyente et al., 2011). The calculated swallowing brain networks were averaged across the conditions for first, second, third, forth, and fifth swallows. Depending on the density levels of connection, the brain networks will have different sparsity. Previous studies have shown that networks with more than 40% of the connection can be considered as too dense (Latora and Marchiori, 2001; Bassett and Bullmore, 2006). Thus, in the formed connectivity matrices we applied a threshold such that we keep 40% of the strongest connections in the network.

The most convenient way to provide signals on graphs is to form a line graph from the original graphs, which corresponds to the synchronization between signals from the EEG electrodes during swallowing (West, 2001). With the newly formed line graphs, the weights of the edges from the original graph will correspond to the nodes of the line graph, while the new nodes will be connected if edges from the original graph that correspond to the vertices of the line graph, are connected to the same node. All connections from the new line graph will have weights equal to one. Thus, we define an undirected, unweighted graph $G = \{\mathcal{V}, \mathcal{W}\}$, where $\mathcal{V}$ is a set of vertices in the graph, and $\mathcal{W}$ is the connectivity matrix of the graph.

Analysis of the differences between conditions

For forming vertex-frequency representations of the swallowing brain networks, we used vertex-invariant optimized $FWGFT$ and vertex-invariant optimized $FGST$. In order to estimate the differences between vertex-frequency representations between consecutive swallows, we calculated the Euclidean distance for each pair of swallows. The Wilcoxon rank-sum statistical test (Wilcoxon et al., 1963) was then used to examine whether the obtained Euclidean distance values between different fluid viscoties are statistically different.

Results

The vertex frequency representations were calculated using 252 saliva swallows, 245 water swallows, 233 nectar-thick liquid swallows, and 228 honey-thick liquid swallows. The results were presented as a vertex frequency representation of the line graph formed from averaged swallowing brain networks for the first, second, third, forth, and fifth swallows during saliva, water, nectar, and honey swallows.

Figure 5 summarizes $FWGFT$ representation of the signals on graphs that correspond to the brain network during consecutive swallowing of various stimuli, while Figure 6 summarizes the $FGST$ representation of the signals on graphs that correspond to the brain network during consecutive swallowing of various stimuli. All vertex-frequency representations have the most dominant energy at the lower frequencies. Also,

each representation shows the frequency burst, which is the most prominent around 300th and around 700th node.

Table 2 summarizes the Euclidean distance for the standard $FWGFT$ and standard $FGST$ between consecutive swallows among various viscosity fluids, while Table 3 summarizes the Euclidean distance for the optimal $FWGFT$ and optimal $FGST$ between consecutive swallows among various viscosities. According to the tables, the mean Euclidean distance between consecutive swallows tends to be lower for thinner liquids. It should be pointed out that the Euclidean distance values for saliva swallows are statistically lower than for other fluid viscosities ($p \ll 0.01$). Also, the values of the Euclidean distance between consecutive swallows for the standard and the optimal representations are very similar.

Discussion

In this paper, we have introduced an algorithm for optimizing the window size for calculating $FWGFT$ and $FGST$. We showed that the optimized window size provided a higher energy concentration for the vertex-frequency representation. In addition, we used this algorithm to investigate differences between signals on the brain networks for consecutive swallows.

From Figures 2 and 3 the improvement of the vertex-frequency representation of the algorithms with optimal window size can be seen. This improvement is confirmed by Table 1, where the results showed a higher performance measure value for the algorithm with the optimized window size. Even though the optimized $FWGFT$ and the optimized $FGST$ have higher energy concentrations for the vertex-frequency representation, these optimized algorithms have a higher computational complexity in comparison with the standard $FWGFT$ and $FGST$. A higher computational complexity resulted from the optimization procedure, which is necessary for the parameter tuning. However, in comparison with the windowed graph Fourier transform and graph S-transform (Shuman et al., 2013b), the optimized $FWGFT$ and the optimized $FGST$ still have a significantly lower computational complexity.

Our hypothesis that the vertex-frequency information of the brain network is different between consecutive swallows is supported by our results. Swallowing is a complex process, which involves the activation of many sensory receptors in the oral cavity, as well as, the activation of several head and neck muscles. Previous studies have shown that changes in EEG wave forms during voluntary movement can be observed in the sensorimotor areas of the cortex. Consecutive swallows can cause neuromuscular fatigue, which can result in a reduced level of muscular force involved in performing this activity (Edwards, 1981). Therefore, the results can be attributed to the changes caused by the activation of the sensorimotor neurons due to neuromuscular fatigue.

Similarity between vertex frequency representation of the brain networks during consecutive swallows tends to be lower for the thicker liquids. Previous studies, which have investigated brain activity during

eating, reported that different groups of neurons are activated due to various food viscosity, or due to the various food taste, or sometimes due to various viscosity and taste combinations (De Araujo and Rolls, 2004). It has also has been reported that some neurons are only activated by specific ranges of fluid viscosities (Rolls et al., 2003). This means that some neurons will have increased or decreased activity due to various viscosities. Also, studies have shown that consuming thicker liquids causes an increase in submental muscles' activity (Reimers-Neils et al., 1994), which increases the traction forces applied to the hyolaryngeal complex leading to airway closure during swallowing and opening of the upper esophageal sphincter. The changes in the muscle activity are controlled by changes in neural activity in the brain (Herrmann and Mecklinger, 2001; Niedermeyer and da Silva, 2005). Increased or decreased neural activity cause changes in EEG waveforms, which will affect the weights of the connection in the swallowing brain network. The changes in the connection weights in the swallowing brain network will directly modulate signals on the line graphs that correspond to the swallowing brain network. Thus, the lower similarity between the vertex frequency representations during consecutive swallows of thicker liquids could be attributed to the changes in the neural responses that the higher viscosity fluids produce.

According to Tables 2 and 3, the Euclidean distance is much smaller for the dry swallows (i.e., saliva swallows) as compared to the wet swallows (i.e., water, nectar-thick, and honey-thick). During swallowing, sensory receptors in the oral cavity capture information about the bolus size, shape, temperature, smell, and taste. The captured information is sent to the sensory motor cortex and a motor plan is produced by the swallowing central pattern generator in the brainstem (Miller, 1999). In the case of saliva swallows, sensory information, such as temperature, smell, and taste, are not captured. Thus, the neurons which are involved in processing this sensory information, will not be activated. Also, this study was conducted such that participants consumed wet stimuli from cups. Consumption of stimuli from cups involves additional head movements, which activate additional neurons that are responsible for motor activation. Thus, a smaller Euclidean distance between vertex-frequency for the consecutive swallows could be attributed to the reduced motor activity and sensory stimulation of the dry swallows.

Figure 5 and 6 show that the vertex-frequency representations of the swallowing brain networks mostly contain low frequency components. In addition, they display the frequency burst around 300th and around 700th node. In the line graph, the connections of the newly formed nodes depend on the position of the edges in the original graph. By applying thresholds on the brain networks, the low connections are dismissed, which disable the direct connection between some neighboring nodes in the line graph. This indirect connection results in more oscillations in the signal between neighboring nodes resulting higher frequency in the vertex-frequency representation. This means that the position of the weak connections and proper thresholding of the brain network can be very important for future studies, as it provides distinctive information about the brain network.

A limitation of this study is that the bolus size was not measured. There is a possibility that a non-uniform bolus size could affect the brain network in different sized subjects. Another limitation is that the order of consumed stimuli was the same for each participant (i.e., saliva first, water second, nectar-thick third, honey-thick forth). The order of consumed stimuli could also potentially influence the results of the formation of brain networks. Thus, future investigations should consider measuring of the bolus size and scaling bolus volume to a standard proportion of bolus volume to patient size, as well as, randomizing the order of consumed stimuli.

Conclusion

In this study, we presented an algorithm, which provides a higher energy concentration of the $FWGFT$ and $FGST$. The algorithm was based on the window size optimization, which uses the concentration measure. In order to optimize the window size with the graph S-transform, we introduced a new parameter, which controls the window size that corresponds to each frequency point. The algorithm was tested using two synthetic signals. The results of the tests showed that the optimized $FWGFT$ and the optimized $FGST$ have a higher energy concentration than $FWGFT$ and $FGST$. In addition, we used the proposed algorithm to investigate differences between consecutive swallows by analyzing vertex-frequency information of the swallowing brain networks. For this analysis, we collected signals from 55 healthy people, who performed five saliva, five water, five nectar thick, and five honey thick swallows. We showed that there are differences in the vertex-frequency representations of the brain networks between consecutive swallows, which can be attributed to changes in activation of the sensorimotor neurons due to fatigue in the muscular force. Furthermore, we showed that differences between consecutive swallows are higher for the thicker liquids, which corresponds to the changes of the cortical activation due to various sensory stimulation.

Acknowledgments

Research reported in this publication was supported by the Eunice Kennedy Shriver National Institute of Child Health & Human Development of the National Institutes of Health under Award Number R01HD074819. The content is solely the responsibility of the authors and does not necessarily represent the official views of the National Institutes of Health.

References

Adnerhill, I., Ekberg, O., and Groher, M. E. (1989). Determining normal bolus size for thin liquids. *Dysphagia*, 4:1–3.

Aviyente, S., Bernat, E. M., Evans, W. S., and Sponheim, S. R. (2011). A phase synchrony measure for quantifying dynamic functional integration in the brain. *Hum Brain Mapp*, 32:80–93.

Aydogdu, I., Ertekin, C., Tarlaci, S., Turman, B., Kiylioglu, N., and Secil, Y. (2001). Dysphagia in lateral medullary infarction (wallenbergs syndrome) an acute disconnection syndrome in premotor neurons related to swallowing activity? *Stroke*, 32:2081–2087.

Bassett, D. S. and Bullmore, E. (2006). Small-world brain networks. *The Neuroscientist*, 12:512–523.

Bhatia, S. J. and Shah, C. (2013). How to perform and interpret upper esophageal sphincter manometry. *Journal of Neurogastroenterology and Motility*, 19:99–103.

Bieger, D. (1993). Central nervous system control mechanisms of swallowing: a neuropharmacological perspective. *Dysphagia*, 8:308–310.

Bryan, C. S. and Reynolds, K. (1984). Bacteremic nosocomial pneumonia. analysis of 172 episodes from a single metropolitan area. *The American Review of Respiratory Disease*, 129:668.

Cichero, J. A. and Murdoch, B. E. (2006). *Dysphagia: foundation, theory and practice*. John Wiley & Sons, New York City, NY.

Curran, J. (1992). Nutritional considerations. *Dysphagia*, pages 255–266.

Curran, J. and Groher, M. E. (1990). Development and dissemination of an aspiration risk reduction diet. *Dysphagia*, 5:6–12.

Davenport, P. W., Bolser, D. C., and Morris, K. F. (2011). Swallow remodeling of respiratory neural networks. *Head Neck*, 33:8–13.

De Araujo, I. E. and Rolls, E. T. (2004). Representation in the human brain of food texture and oral fat. *The Journal of Neuroscience*, 24:3086–3093.

Delorme, A. and Makeig, S. (2004). EEGLAB: an open source toolbox for analysis of single-trial EEG dynamics including independent component analysis. *J Neurosci Methods*, 134:9–21.

Doeltgen, S. H. and Huckabee, M.-L. (2012). Swallowing neurorehabilitation: from the research laboratory to routine clinical application. *Arch Phys Med Rehabil*, 93:207–213.

Dusick, A. (2003). Investigation and management of dysphagia. In *Seminars in Pediatric Neurology*, volume 10, pages 255–264. Elsevier.

Eberle, W. and Holder, L. (2007). Anomaly detection in data represented as graphs. *Intelligent Data Analysis*, 11:663–689.

Edwards, R. H. (1981). Human muscle function and fatigue. In *Human muscle fatigue: physiological mechanisms*, volume 82, pages 1–18. Pitman Medical London.

Eguiluz, V. M., Chialvo, D. R., Cecchi, G. A., Baliki, M., and Apkarian, A. V. (2005). Scale-free brain functional networks. *Phys Rev Lett*, 94:018102.

Eisbruch, A., Lyden, T., Bradford, C. R., Dawson, L. A., Haxer, M. J., Miller, A. E., Teknos, T. N., Chepeha, D. B., Hogikyan, N. D., Terrell, J. E., and Wolf, G. T. (2002). Objective assessment of swallowing dysfunction and aspiration after radiation concurrent with chemotherapy for head-and-neck cancer. *Int J Radiat Oncol Biol Phys*, 53:23–28.

Garibaldi, R. A., Brodine, S., and Matsumiya, S. (1981). Infections among patients in nursing homes: policies, prevalence, problems. *The New England Journal of Medicine*, 305:731.

Garrett, D. D., Kovacevic, N., McIntosh, A. R., and Grady, C. L. (2012). The modulation of bold variability between cognitive states varies by age and processing speed. *Cerebral Cortex*, 23:684–693.

Gottlieb, D., Kipnis, M., Sister, E., Vardi, Y., and Brill, S. (1996). Validation of the 50 ml3 drinking test for evaluation of post-stroke dysphagia. *Disabil Rehabil*, 18:529–532.

Hamdy, S., Rothwell, J. C., Aziz, Q., and Thompson, D. G. (2000). Organization and reorganization of human swallowing motor cortex: implications for recovery after stroke. *Clin Sci*, 99:151–157.

Hammond, D. K., Vandergheynst, P., and Gribonval, R. (2011). Wavelets on graphs via spectral graph theory. *Appl Comput Harmon Anal*, 30:129–150.

Heisz, J. J., Shedden, J. M., and McIntosh, A. R. (2012). Relating brain signal variability to knowledge representation. *Neuroimage*, 63:1384–1392.

Herrmann, C. S. and Mecklinger, A. (2001). Gamma activity in human EEG is related to highspeed memory comparisons during object selective attention. *Visual Cognition*, 8:593–608.

Hyvärinen, A. and Oja, E. (2000). Independent component analysis: algorithms and applications. *Neural Networks*, 13:411–430.

Jasper, H. H. (1958). The ten twenty electrode system of the international federation. *Electroencephalogr Clin Neurophysiol*, 10:371–375.

Jestrović, I., Coyle, J., and Sejdić, E. (2017). A fast algorithm for vertex-frequency representations of signals on graphs. *Signal Process*, 131:483–491.

Jestrović, I., Coyle, J. L., and Sejdić, E. (2015). Decoding human swallowing viaelectroencephalography: a state-of-the-artreview. *J Neural Eng*, 12:1–15.

Jestrović, I., Dudik, J. M., Luan, B., Coyle, J. L., and Sejdić, E. (2013). The effects of increased fluid viscosity on swallowing sounds in healthy adults. *Biomed Eng Online*, 12:90–107.

Kaiser, M. and Hilgetag, C. C. (2004). Edge vulnerability in neural and metabolic networks. *Biol Cybern*, 90:311–317.

Langmore, S. E., Terpenning, M. S., Schork, A., Chen, Y., Murray, J. T., Lopatin, D., and Loesche, W. J. (1998). Predictors of aspiration pneumonia: how important is dysphagia? *Dysphagia*, 13:69–81.

Latora, V. and Marchiori, M. (2001). Efficient behavior of small-world networks. *Phys Rev Lett*, 87:198701.

Lazarus, C. and Logemann, J. (1987). Swallowing disorders in closed head trauma patients. *Arch Phys Med Rehabil*, 68:79–84.

Leonardi, N. and Van De Ville, D. (2013). Tight wavelet frames on multislice graphs. *IEEE Trans Signal Process*, 61:3357–3367.

Logemann, J. A. (1998). *Evaluation and treatment of swallowing disorders*. PRO-ED, Incorporated, Austin, TX.

Micheloyannis, S., Pachou, E., Stam, C. J., Vourkas, M., Erimaki, S., and Tsirka, V. (2006). Using graph theoretical analysis of multi channel EEG to evaluate the neural efficiency hypothesis. *Neurosci Lett*, 402:273–277.

Miller, A. J. (1986). Neurophysiological basis of swallowing. *Dysphagia*, 1:91–100.

Miller, A. J. (1999). *The neuroscientific principles of swallowing and dysphagia*. Singular Publishing Group San Diego, San Diego, CA.

Molfenter, S. M. and Steele, C. M. (2013). The relationship between residue and aspiration on the subsequent swallow: an application of the normalized residue ratio scale. *Dysphagia*, 28:494–500.

Murray, J. (1999). *Manual of dysphagia assessment in adults*. Singular, San Diego, CA.

Narang, S. K. and Ortega, A. (2012). Perfect reconstruction two-channel wavelet filter banks for graph structured data. *IEEE Trans Signal Process*, 60:2786–2799.

Narang, S. K. and Ortega, A. (2013). Compact support biorthogonal wavelet filterbanks for arbitrary undirected graphs. *IEEE Trans Signal Process*, 61:4673–4685.

Ney, D. M., Weiss, J. M., Kind, A. J., and Robbins, J. (2009). Senescent swallowing: impact, strategies, and interventions. *Nutr Clin Pract*, 24:395–413.

Niedermeyer, E. and da Silva, F. L. (2005). *Electroencephalography: basic principles, clinical applications, and related fields*. Lippincott Williams & Wilkins, Philadelphia, PA.

Noble, C. C. and Cook, D. J. (2003). Graph-based anomaly detection. In *Proceedings of the ninth ACM SIGKDD international conference on Knowledge discovery and data mining*, pages 631–636. ACM.

Plaxico, D. T. and Loughlin, G. M. (1981). Nasopharyngeal reflux and neonatal apnea: their relationship. *Am J Dis Child*, 135:793–794.

Pugliese, G. and Lichtenberg, D. A. (1987). Nosocomial bacterial pneumonia: an overview. *Am J Infect Control*, 15:249–265.

Ramsey, D. J., Smithard, D. G., and Kalra, L. (2003). Early assessments of dysphagia and aspiration risk in acute stroke patients. *Stroke*, 34:1252–1257.

Reimers-Neils, L., Logemann, J., and Larson, C. (1994). Viscosity effects on EMG activity in normal swallow. *Dysphagia*, 9:101–106.

Robbins, J., Butler, S. G., Daniels, S. K., Gross, R. D., Langmore, S., Lazarus, C. L., Martin-Harris, B., McCabe, D., Musson, N., and Rosenbek, J. (2008). Swallowing and dysphagia rehabilitation: translating principles of neural plasticity into clinically oriented evidence. *J Speech Lang Hear Res*, 51:276–300.

Robbins, J. and Levine, R. L. (1988). Swallowing after unilateral stroke of the cerebral cortex: preliminary experience. *Dysphagia*, 3:11–17.

Rogers, B., Arvedson, J., Buck, G., Smart, P., and Msall, M. (1994). Characteristics of dysphagia in children with cerebral palsy. *Dysphagia*, 9:69–73.

Rolls, E. T., Verhagen, J. V., and Kadohisa, M. (2003). Representations of the texture of food in the primate orbitofrontal cortex: neurons responding to viscosity, grittiness, and capsaicin. *J Neurophysiol*, 90:3711–3724.

Rosenkranz, K., Butler, K., Williamon, A., Cordivari, C., Lees, A., and Rothwell, J. (2008). Sensorimotor reorganization by proprioceptive training in musician's dystonia and writer's cramp. *Neurology*, 70:304–315.

Sang, Q. and Goyal, R. K. (2001). Swallowing reflex and brain stem neurons activated by superior laryngeal nerve stimulation in the mouse. *American Journal of Physiology-Gastrointestinal and Liver Physiology*, 280:191–200.

Sejdić, E., Djurović, I., and Jiang, J. (2008). A window width optimized S-transform. *EURASIP Journal on Advances in Signal Processing*, 2008:59–72.

Sejdić, E., Djurović, I., and Jiang, J. (2009). Time-frequency feature representation using energy concentration: An overview of recent advances. *Digital Signal Processing*, 19(1):153–183.

Shuman, D. I., Narang, S. K., Frossard, P., Ortega, A., and Vandergheynst, P. (2013a). The emerging field of signal processing on graphs: Extending high-dimensional data analysis to networks and other irregular domains. *IEEE Signal Proc Mag*, 30:83–98.

Shuman, D. I., Ricaud, B., and Vandergheynst, P. (2013b). Vertex-frequency analysis on graphs. *Appl Comput Harmon Anal*, 40:206–291.

Smithard, D., O'Neill, P., Park, C., Morris, J., Wyatt, R., England, R., and Martin, D. (1996). Complications and outcome after acute stroke. Does dysphagia matter? *Stroke*, 27:1200–1204.

Solomon, N. P. (2006). What is orofacial fatigue and how does it affect function for swallowing and speech? In *Seminars in Speech and Language*, volume 27, page 268. NIH Public Access.

Sporns, O. and Zwi, J. D. (2004). The small world of the cerebral cortex. *Neuroinformatics*, 2:145–162.

Stanković, L. (2001). A measure of some time–frequency distributions concentration. *Signal Process*, 81:621–631.

Sun, J., Qu, H., Chakrabarti, D., and Faloutsos, C. (2005). Neighborhood formation and anomaly detection in bipartite graphs. In *Fifth IEEE International Conference on Data Mining*, pages 8–pp. IEEE.

Veis, S. and Logemann, J. (1985). Swallowing disorders in persons with cerebrovascular accident. *Arch Phys Med Rehabil*, 66:372–375.

West, D. B. (2001). *Introduction to graph theory*, volume 2. Prentice hall Upper Saddle River, Upper Saddle River, NJ.

Wilcoxon, F., Katti, S., and Wilcox, R. A. (1963). *Critical values and probability levels for the Wilcoxon rank sum test and the Wilcoxon signed rank test.* American Cyanamid Company, New York City, NY.

Table captions

Table 1 - Performance measure values for the considered vertex-frequency representations.

Table 2 - Root mean squared difference values (mean ± standard error) for the standard $FWGFT$ and standard $FGST$ between consecutive swallows.

Table 3 - Root mean squared difference values (mean ± standard error) for the optimal $FWGFT$ and optimal $FGST$ between consecutive swallows.

Tables

Table 1

	Noise free		SNR=20dB		SNR=10dB	
	Ξ_{s1}	Ξ_{s2}	Ξ_{s1}	Ξ_{s2}	Ξ_{s1}	Ξ_{s2}
Standard $WGFT$	0.0096	0.0093	0.0071	0.0070	0.0063	0.0063
Vertex-invariant optimized $FWGFT$	0.0097	0.0093	0.0073	0.0072	0.0064	0.0064
Vertex dependent optimized $FWGFT$	0.0097	0.0093	0.0091	0.0090	0.0081	0.0081
Standard $FGST$	0.0086	0.0081	0.0071	0.0068	0.0065	0.0066
Vertex-invariant optimized $FGST$	0.0094	0.0089	0.0073	0.0070	0.0068	0.0068
Vertex dependent optimized $FGST$	0.0096	0.0088	0.0092	0.0086	0.0080	0.0077

Table 2

Swallows comparison	Standard $FWGFT$				Standard $FGST$			
	Saliva	Water	Nectar	Honey	Saliva	Water	Nectar	Honey
1-2	8.45 ± 0.09	12.8 ± 0.09	13.2 ± 0.12	13.3 ± 0.12	9.24 ± 0.09	13.8 ± 0.09	14.2 ± 0.12	14.3 ± 0.12
1-3	8.18 ± 0.07	12.8 ± 0.08	13.2 ± 0.13	13.4 ± 0.10	8.89 ± 0.08	13.8 ± 0.08	14.3 ± 0.13	14.3 ± 0.09
1-4	8.39 ± 0.08	12.3 ± 0.08	13.1 ± 0.12	13.0 ± 0.10	9.15 ± 0.08	13.4 ± 0.08	14.0 ± 0.11	14.0 ± 0.10
1-5	7.99 ± 0.06	12.3 ± 0.08	12.5 ± 0.11	13.0 ± 0.10	8.72 ± 0.07	13.3 ± 0.08	13.5 ± 0.11	14.0 ± 0.10
2-3	8.56 ± 0.10	12.9 ± 0.08	13.3 ± 0.13	13.3 ± 0.10	9.31 ± 0.10	13.9 ± 0.08	14.5 ± 0.14	14.2 ± 0.10
2-4	8.78 ± 0.10	12.5 ± 0.08	13.2 ± 0.12	12.8 ± 0.11	9.61 ± 0.10	13.5 ± 0.08	14.2 ± 0.12	13.9 ± 0.11
2-5	8.36 ± 0.09	12.4 ± 0.08	12.6 ± 0.12	12.8 ± 0.11	9.17 ± 0.09	13.4 ± 0.08	13.7 ± 0.12	13.9 ± 0.11
3-4	8.48 ± 0.09	12.3 ± 0.07	13.3 ± 0.13	12.9 ± 0.09	9.25 ± 0.10	13.4 ± 0.08	14.3 ± 0.13	14.0 ± 0.09
3-5	8.11 ± 0.08	12.3 ± 0.07	12.8 ± 0.12	12.9 ± 0.09	8.82 ± 0.08	13.3 ± 0.07	13.9 ± 0.12	13.9 ± 0.09
4-5	8.31 ± 0.08	11.8 ± 0.07	12.5 ± 0.11	12.5 ± 0.09	9.11 ± 0.08	12.9 ± 0.07	13.6 ± 0.11	13.6 ± 0.09

Table 3

Swallows comparison	Optimal $FWGFT$				Optimal $FGST$			
	Saliva	Water	Nectar	Honey	Saliva	Water	Nectar	Honey
1-2	7.81 ± 0.08	11.9 ± 0.10	12.1 ± 0.13	12.5 ± 0.13	9.19 ± 0.08	13.7 ± 0.09	14.1 ± 0.12	14.2 ± 0.11
1-3	7.63 ± 0.07	11.8 ± 0.08	12.2 ± 0.14	12.5 ± 0.11	8.85 ± 0.08	13.7 ± 0.08	14.2 ± 0.13	14.3 ± 0.09
1-4	7.82 ± 0.08	11.2 ± 0.09	12.2 ± 0.09	12.2 ± 0.11	9.11 ± 0.08	13.3 ± 0.08	14.0 ± 0.11	13.9 ± 0.10
1-5	7.41 ± 0.06	11.3 ± 0.08	11.4 ± 0.12	11.9 ± 0.11	8.68 ± 0.07	13.2 ± 0.08	13.4 ± 0.11	13.9 ± 0.10
2-3	7.96 ± 0.10	11.9 ± 0.09	12.2 ± 0.14	12.3 ± 0.11	9.26 ± 0.10	13.8 ± 0.08	14.3 ± 0.13	14.1 ± 0.10
2-4	8.16 ± 0.09	11.5 ± 0.09	12.3 ± 0.13	11.9 ± 0.12	9.56 ± 0.10	13.4 ± 0.08	14.1 ± 0.12	13.8 ± 0.11
2-5	7.73 ± 0.08	11.5 ± 0.09	11.5 ± 0.13	11.8 ± 0.12	9.12 ± 0.09	13.3 ± 0.08	13.6 ± 0.12	13.8 ± 0.11
3-4	7.92 ± 0.08	11.2 ± 0.08	12.3 ± 0.14	11.9 ± 0.09	9.20 ± 0.09	13.3 ± 0.08	14.2 ± 0.13	13.9 ± 0.09
3-5	7.54 ± 0.08	11.3 ± 0.08	11.6 ± 0.13	11.8 ± 0.10	8.77 ± 0.08	13.2 ± 0.07	13.8 ± 0.12	13.8 ± 0.09
4-5	7.72 ± 0.07	10.7 ± 0.08	11.5 ± 0.12	11.4 ± 0.10	9.06 ± 0.08	12.8 ± 0.08	13.5 ± 0.11	13.5 ± 0.09

Figure captions

Figure 1: Test signals used for the theoretical analysis of the proposed algorithm. These test signals are non-stationary signals that can depict time-varying brain networks. (A) depicts s_1, while (B) depicts s_2.

Figure 2: Vertex-frequency representations for the test signal s_1. Optimized representations exhibit more localized representations in the vertex-frequency domain. (A) Standard FWGFT; (B) Optimized FWGFT; (C) Vertex-optimized FWGFT; (D) Standard FGST; (E) Optimized FGST; (F) Vertex-optimized FGST.

Figure 3: Vertex-frequency representations for the test signal s_2. Similarly to representations obtained for s_1, optimized representations provide more localized vertex-frequency distributions. (A) Standard FWGFT; (B) Optimized FWGFT; (C) Vertex-optimized FWGFT; (D) Standard FGST; (E) Optimized FGST; (F) Vertex-optimized FGST.

Figure 4: The experimental procedure used in this study. EEG electrodes were positioned according to the 10-20 international electrode system, while the dual-axis accelerometer was positioned on the anterior side of the participant's neck.

Figure 5: The vertex frequency representation of the brain network during consecutive saliva (A), water (B), nectar (C), and honey (D) swallows using $FWGFT$.

Figure 6: The vertex frequency representation of the brain network during consecutive saliva (A), water (B), nectar (C), and honey (D) swallows using $FGST$. Very strong vertex-frequency components can be observed in these graphs.

Figure 1

Click here to download high resolution image

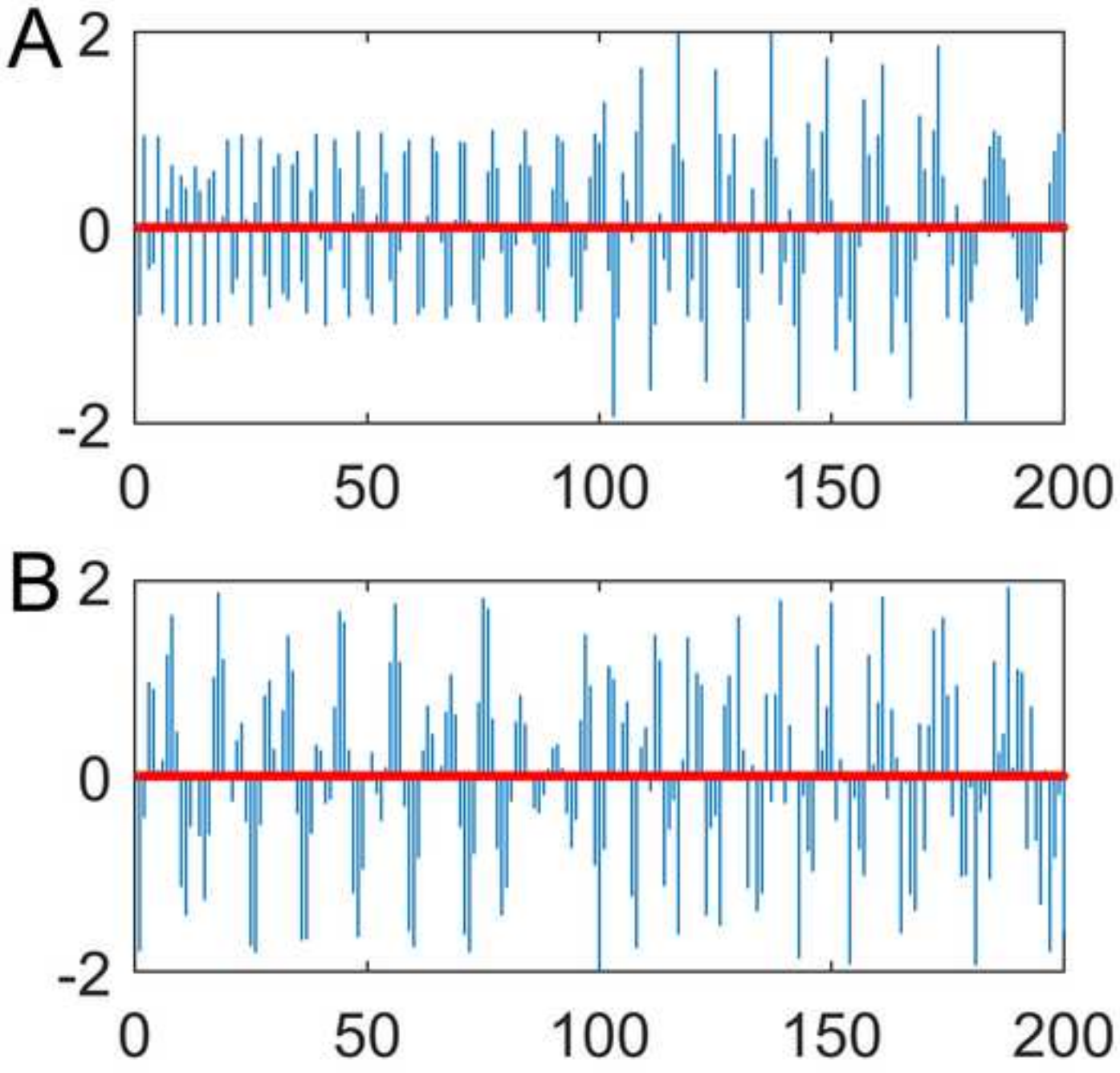

Figure 2

Click here to download high resolution image

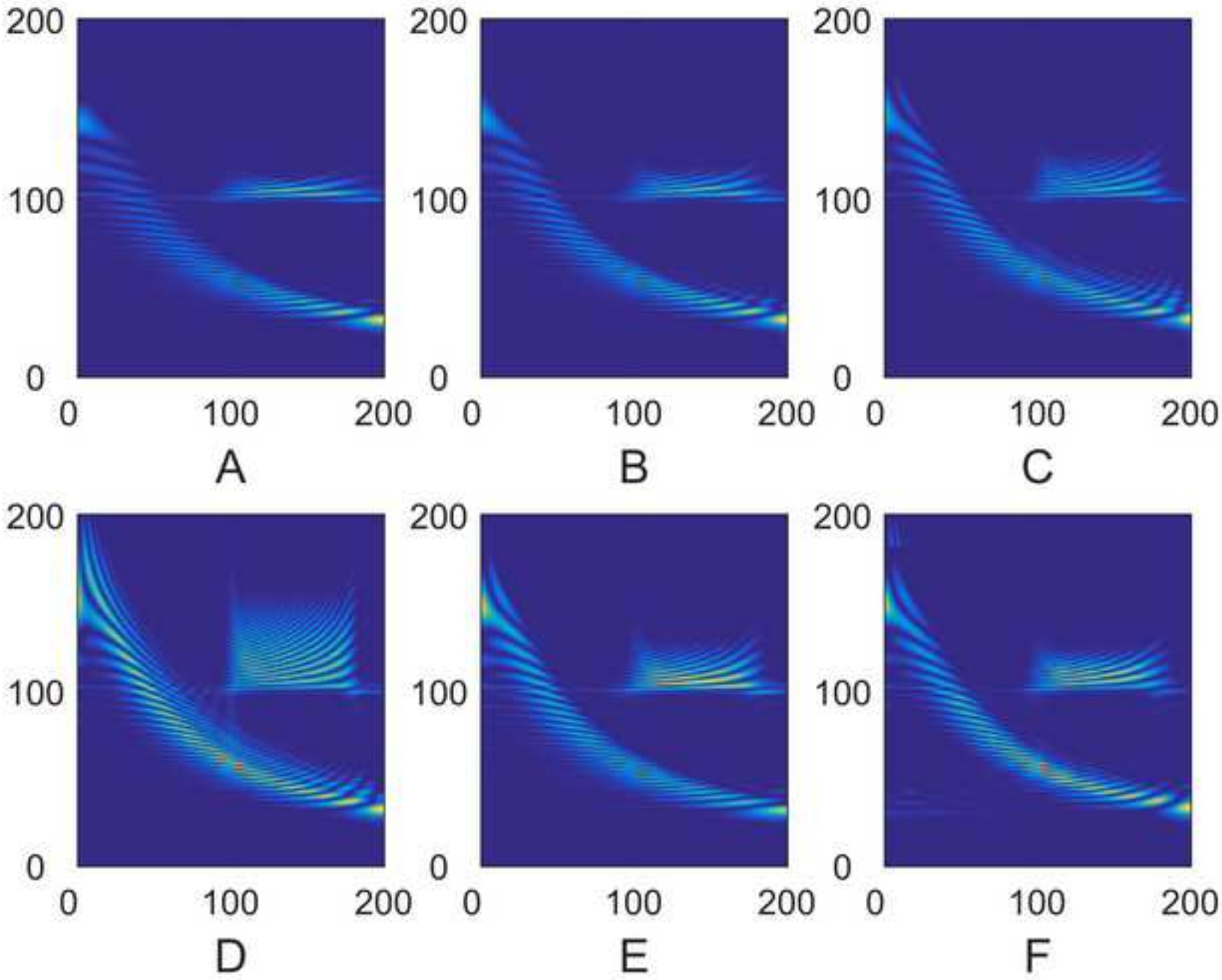

Figure 3

Click here to download high resolution image

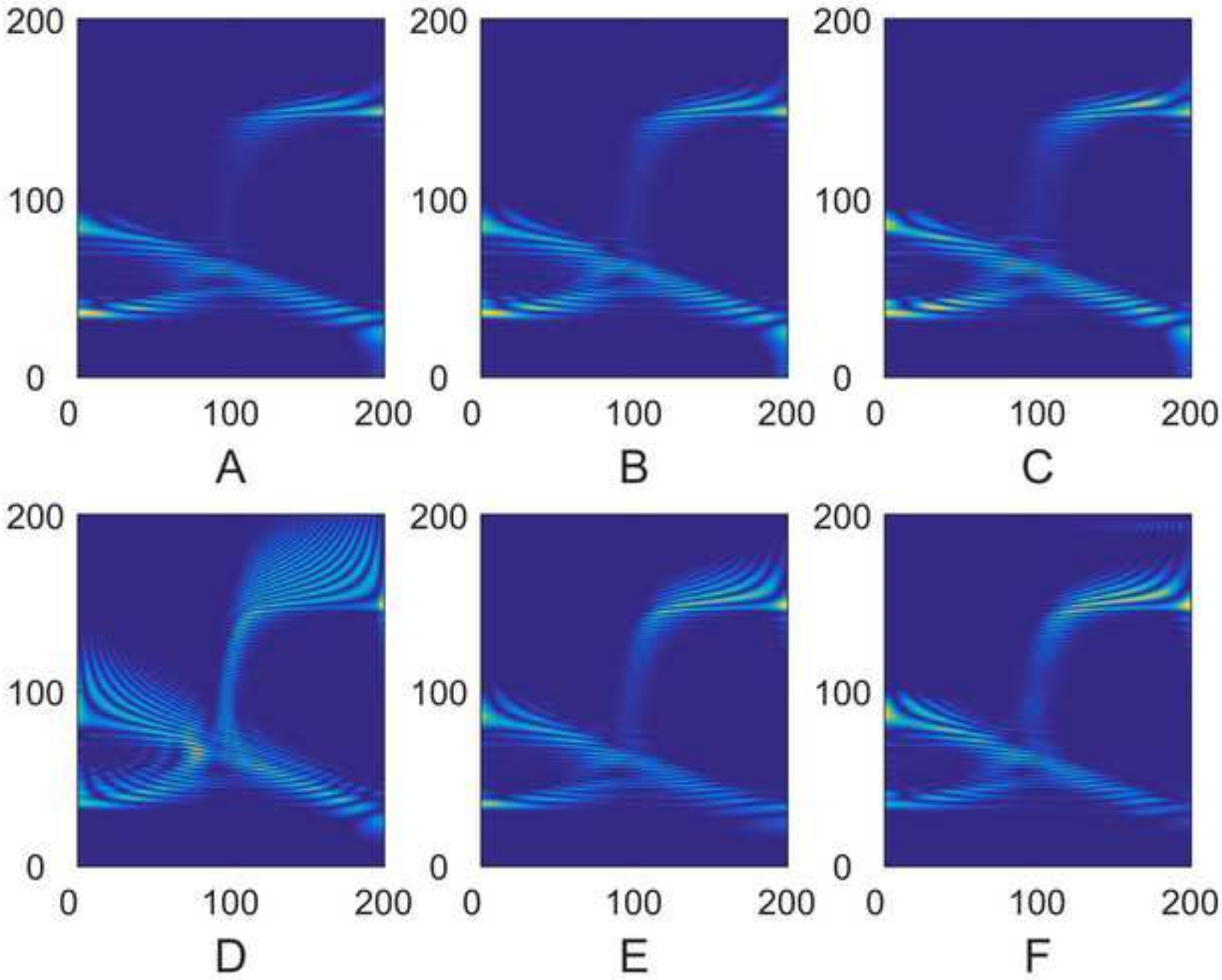

Figure 4

Click here to download high resolution image

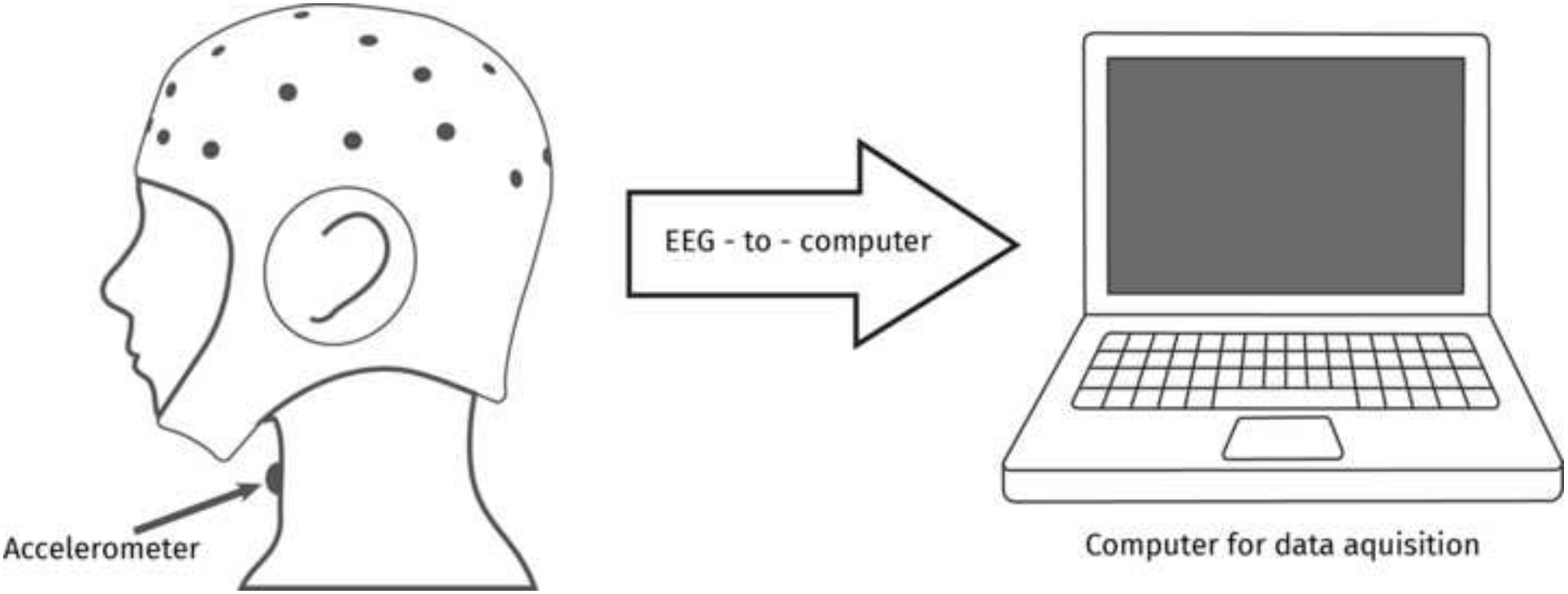

Figure 5

Click here to download high resolution image

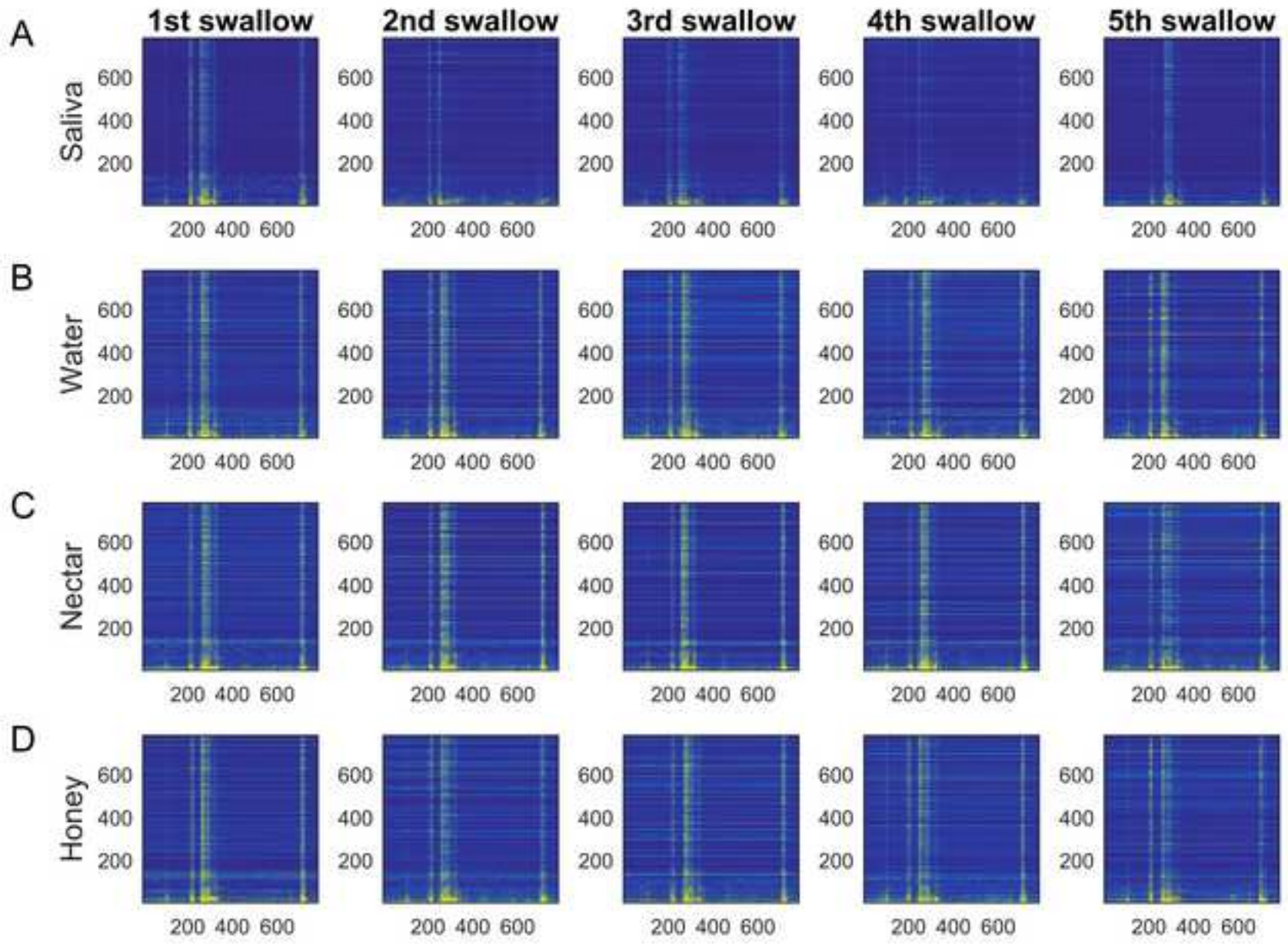

Figure 6

Click here to download high resolution image